11-1-2000

Secular Variations of Atomic Oxygen in the Mesopause Region Induced by Transient Gravity Wave Packets

Michael P. Hickey Ph.D.
Embry-Riddle Aeronautical University, hicke0b5@erau.edu

R. L. Walterscheid
The Aerospace Corporation

Philip G. Richards
University of Alabama - Huntsville

Scholarly Commons Citation

Geophysical Research Letters, vol. 27, no. 21, pages 3599-3602, November 1, 2000.

GEOPHYSICAL RESEARCH LETTERS, VOL. 27, NO. 21, PAGES 3599-3602, NOVEMBER 1, 2000

Secular Variations of Atomic Oxygen in the Mesopause Region Induced by Transient Gravity Wave Packets

Michael P. Hickey

Department of Physics and Astronomy, Clemson University, Clemson SC 29634-0978

Richard L. Walterscheid

Space Science Applications Laboratory, The Aerospace Corporation, Los Angeles, CA 90009

Philip G. Richards

Computer Science Department and Center for Space Plasma, Aeronomy, and Astrophysics Research, The University of Alabama in Huntsville, Huntsville AL 35899

Abstract. We employ a 2-dimensional, time-dependent, fully nonlinear model of minor species in the mesopause region and our Spectral Full-Wave Model to simulate the response of atomic oxygen (O) to a gravity wave packet in the mesopause region. We demonstrate that gravity waves affect the time-averaged distribution of O in the mesosphere and lower thermosphere (MLT) region through the constituent fluxes the waves induce. Our conclusions are based on simulations of two wave packets that violate the non-acceleration conditions through transience and dissipation. The net cycle-averaged effect of the waves is to significantly increase (by as much as 50%) the O density through downward transport of O at low altitudes (≤ 90 km), and to deplete (by as much as 20%) the O density above ~ 100 km altitude. Comparison with results obtained including only chemistry and diffusion suggests that the effects of gravity wave transport on the distribution of O in this region can be greater than the effects of eddy transport.

1.0 Introduction

Atomic oxygen (O) plays a central role in the chemistry of the mesosphere, lower thermosphere (MLT) region. Both chemical and dynamical processes determine its height distribution. Its chemical lifetime varies from about a day near 80 km altitude to a week at 100 km [e.g., *Torr*, 1985]. It is produced in the thermosphere and upper mesosphere through the dissociation of O_2, and transported downwards from the lower thermosphere into the upper mesosphere by molecular and eddy diffusion, wave transport, and the mean meridional circulation. Usually, the wave transport of minor constituents, which is the subject of this paper, is not considered.

Studies describing the effects of linear gravity waves on minor species in the MLT region have either employed linear, steady-state chemistry in order to quantify wave effects [e.g., *Walterscheid and Schubert*, 1989; *Hickey et al.*, 1993; *Schubert et al.*, 1991; *Hickey et al.*, 1997], or have parameterized the effects of the waves on the chemistry [e.g., *Strobel*, 1981; *Schoeberl et al.*, 1983; *Garcia and Solomon*, 1985; *Gardner and Zhao*, 2000]. *Walterscheid and Schubert* [1989] demonstrated that linear gravity waves can cause a net cycle-averaged (i.e., averaged over a complete wave period) transport of chemically active minor species having time constants that are not large compared to a wave period. Their linear, conservative, steady-state model predicted no significant net cycle-averaged transport for O because of its very long chemical lifetime. *Gardner and Zhao* [2000] used *Weinstock's* [1984] parameterization to demonstrate that gravity waves cause a flux of O. However, implicit in Weinstock's parameterization is the nonlinearity of the wave field, due to wave-wave interactions or associated with wave breakdown. This transport is different from the transport due to cycle-averaged wave fluxes we consider here.

We demonstrate that in the MLT region, gravity waves can cause a net cycle-averaged transport of minor species having long chemical lifetimes, such as O. Mean state forcing is expected whenever the non-acceleration conditions are violated. These conditions are that the waves be linear, conservative, steady, and not encounter a critical level [*Eliasesen and Palm*, 1961; *Andrews and McIntyre*, 1976; *Walterscheid*, 1995]. In addition, transport will occur whenever chemistry is able to induce an out of quadrature relation between the vertical velocity and mixing ratio fluctuations. This process is not effective for the waves considered here for O because of its long chemical time constant compared to the dynamical time constants. For the first time a rigorous modeling approach is applied to the problem of calculating O fluxes driven by the combined effects of gravity wave transience and dissipation. Using a 2-D, time-dependent, fully nonlinear model describing the response of minor species in the mesopause region to dynamical forcing by a gravity wave packet, we demonstrate the important role of gravity wave packets in the distribution of O in the MLT region.

2.0 Model

We model the forcing influence of a gravity wave packet (simulated with our Spectral Full-Wave Model) on minor species in the MLT region (simulated with a time-dependent, fully nonlinear chemistry model), as described next.

2.1 Spectral Full-Wave Model

The Spectral Full-Wave Model (SFWM) simulates a time-dependent wave packet using a spectral approach. A full-

Paper number 2000GL011953.
0094-8276/00/2000GL011953$05.00

wave model [*Hickey et al.*, 1997, 1998, 2000] provides solutions to the Navier-Stokes equations for monochromatic, linear waves propagating in a non-isothermal atmosphere including the effects of the eddy and molecular diffusion of heat and momentum and the Coriolis force. The inhomogeneous forcing term in the energy equation has the form $F(t) = \exp[-(t-\tau)^2/\Delta t^2]\sin(\omega_0 t - k_0 x)$, where ω_0 and k_0 are frequency and horizontal wavenumber of the forcing wave, and where the Gaussian envelope is centered on time $t = \tau$, with a half width of $2\Delta t$. The altitude profile of the forcing is a Gaussian of half-width 0.125 km centered on 10 km altitude. A numerical Fourier transform of $F(t)$ gives the spectrum, $G(\omega,k)$. Because the packet is only localized in time and altitude, the k dependence of G is a delta function, $\delta(k-k_0)$. With the forcing specified by $G(\omega,k)$, the full-wave calculation for the (ω,k) pair provides $u'(\omega,k,z)$, $w'(\omega,k,z)$, $T'(\omega,k,z)$, and $\rho'(\omega,k,z)$ (written as $\psi'(\omega,k,z)$). The SFWM provides $u'(x,z,t)$, $w'(x,z,t)$, $T'(x,z,t)$, and $\rho'(x,z,t)$ (written as $\Psi'(x,z,t)$) using the inverse Fourier transform

$$\Psi'(x,z,t) = \int_{-\infty}^{\infty}\int_{-\infty}^{\infty} \psi'(\omega,k,z) e^{i(\omega t - kx)}\, d\omega\, dk \qquad (1)$$

We evaluate (1) numerically using 2000 waves (500 positive and 500 negative ω, and 1 positive and 1 negative k). The forcing period is 20 minutes. The periods used in (1) range from ~5 minutes to ~40 hours. Here, ω is the wave frequency, k is the horizontal wavenumber, z is altitude, u' and w' are the horizontal and vertical perturbation velocity, respectively, T' is the perturbation temperature, and ρ' is the perturbation density. The amplitude at the forcing frequency is set to a maximum allowed by the *Orlanski and Bryan* [1969] condition just above the main airglow region (~ 110 km).

2.2 Time-Dependent, Nonlinear, 2-D Chemistry Model

Our 2-D, time-dependent, nonlinear chemistry model solves the coupled continuity equations for several minor species (O, $O_2(c^1\Sigma_u^-)$, and $O(^1S)$) including the effects of advection and diffusion, which for a single species is written as

$$\frac{\partial n_i}{\partial t} = P_i - n_i L_i - \underline{\nabla}\cdot\underline{\varphi}_i \qquad (2)$$

where the number density flux ($\underline{\varphi}_i$) is $\underline{\varphi}_i = n_i \underline{v}_i$ and where $\underline{v}_i = \underline{v}' + \overline{\underline{v}}_E + \underline{v}_m + \underline{v}_e$.

Secular variations in constituent concentration induced by wave transport are driven by terms like $\partial \overline{n_i' w'}/\partial z$ arising from the last term in (2), where the overbar denotes an x-t average. Here, n_i are minor species number density, P_i and L_i are chemical production and loss, respectively, $\underline{v}'$ is the wave perturbation velocity, $\overline{\underline{v}}_E$ is the Eulerian mean velocity, $\underline{v}_m$ is the molecular diffusion velocity, and $\underline{v}_e$ is the eddy diffusion velocity. Equations for the diffusion velocities are taken from *Banks and Kockarts* [1973]. The Eulerian-mean velocity ($\overline{\underline{v}}_E$) ensures that the Lagrangian mean displacement is zero when the non-acceleration conditions apply [*Walterscheid and Hocking*, 1991], and is defined by $\overline{w}_e = -\overline{\rho' w'}/\overline{\rho}$.

We use a time-splitting technique to solve (2), which can be written in vector form as $\partial \underline{n}/\partial t = \underline{f}_i(\underline{n}) + \underline{f}_e(\underline{n})$, where subscripts i and e refer to implicit and explicit, respectively. All chemistry terms and those associated with the vertical advection of minor species are solved using a fully implicit Newton's method, while terms associated with horizontal fluxes and other vertical fluxes are solved using the explicit Lax-Wendroff method [*Burstein*, 1967]. The chemical terms in (2) are calculated using the chemical kinetic parameters given by *Hickey and Walterscheid* [1999].

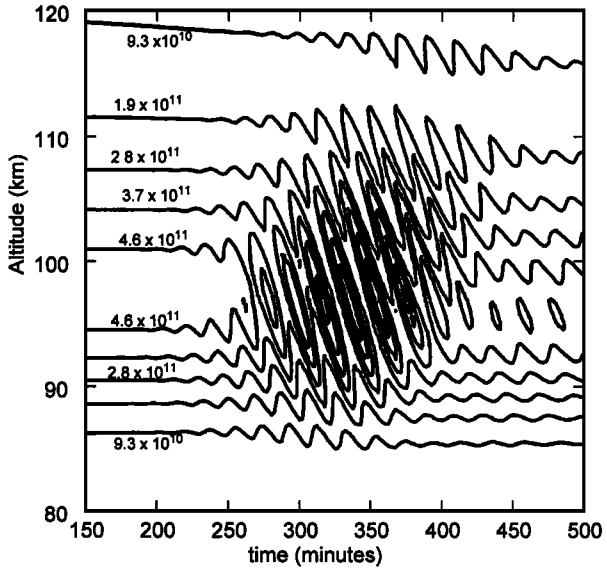

Figure 1. O density response to wave 1 as a function of altitude and time at the first horizontal grid position.

At the lower boundary (75 km) minor species number densities remain constant, and at the upper boundary (135 km) the species are in diffusive equilibrium. We employ periodic lateral boundary conditions by separating the lateral boundaries by a distance of a horizontal wavelength (λ_x) and by requiring that $\Psi'(0,z,t)$ equals $\Psi'(\lambda_x,z,t)$. A time step of 3 seconds, a constant vertical grid spacing of 0.1 km, and a horizontal grid spacing of either 0.5 km or 1 km (corresponding to 60 points in the horizontal direction), provides convergent results.

3.0 Results

We perform experiments using two different wave packets, both characterized by the same frequency spectrum and forcing frequency, but having different values of λ_x: λ_x = 30 km (denoted wave 1) and λ_x = 60 km (denoted wave 2), respectively. The packet parameters are τ = 100 minutes and Δt = 20 minutes. Wave 2 has twice the phase and group velocity of wave 1, and so propagates from the source (at 10 km altitude) to the airglow region (~ 90 km altitude) in a much shorter time (by ~ 1 hr). We therefore present simulation results for times starting at 1.5 hr for wave 2, and at 2.5 hr for wave 1. The eddy diffusion profile used in the SFWM to damp the waves is based on a profile given by *Strobel* [1989], and has a maximum value of 100 $m^2\ s^{-1}$ at 90 km altitude and a full-width at half-maximum of 20 km. In order to isolate wave effects on the secular variations of O, the nominal maximum value of eddy diffusion was 1 $m^2\ s^{-1}$ in the chemistry model.

Altitude profiles of the forcing wave amplitudes (not shown) are characterized by an increase of amplitude with height up to ~104 km and ~120 km for waves 1 and 2, respectively, and then a decrease of amplitude at greater heights due to dissipation. The actual magnitudes of the waves are based on the *Orlanski and Bryan* [1969] condition, as previously stated. Significantly, wave 1 is strongly damped in the

vicinity of the O peak near 100 km altitude, whereas wave 2 is damped at altitudes appreciably higher than the O peak.

Figure 1 shows the response of the O number density to wave 1 as a function of altitude and time. The phase front slopes are consistent with upward energy propagation. The maximum initial value of n(O) is 5.1 x 10^{11} cm^{-3} at 97.6 km altitude. At $t \sim 200$ min the wave packet begins to perturb O near 85 km altitude. Significant perturbations in O occur near the O peak for times around 250 min. Maximum perturbations in n(O) (~70 %) occur in the 97 km region at $t \sim 350$ min.

Figure 2a shows the density variations associated with wave 1 at z = 100 km and at the first horizontal grid position as a function of time. The relative density perturbation of the major gas ($|\rho'|/\bar{\rho}$) is shown as the solid curve, and scaled to the right hand axis. $|\rho'|/\bar{\rho}$ peaks at about 350 minutes with a value of almost 2 %. The initial part of the disturbance ($t \leq$ 350 min) is characterized by amplitude increasing with time, and is associated with the faster Fourier components of the packet. For $t \geq 430$ minutes, the amplitude appears to become constant. Although this part of the wave packet, consisting of the slower Fourier components, decays slowly, it decreases at much greater times (not shown).

The O number density has a fluctuating part and a secular variation, separated as follows. A running average over time is calculated using a window length equal to the forcing period (20 min), and then normalized with respect to the initial value of n(O). This is the relative secular variation, hereafter simply referred to as the secular variation. The difference between n(O) and the running average previously calculated is the fluctuating part, which is normalized to the initial value of n(O) and referred to as the relative O fluctuation.

Figure 2a reveals a secular decrease with increasing time for n(O) (short dashed curve). This decrease is associated with wave transport due to the combined effects of transience and dissipation. Relative fluctuations in n(O) (long-dashed curve) are large (~ 50 %), and in approximate phase quadrature with major gas density fluctuations. Note that at other horizontal (x) grid positions the relative fluctuations in n(O) will have

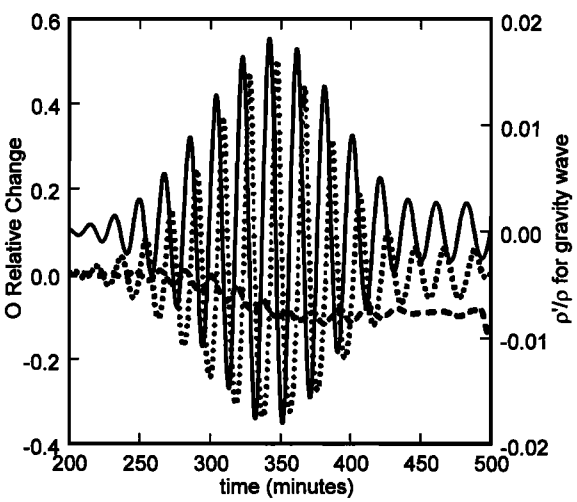

Figure 2a. Relative density perturbations of major gas ($|\rho'|/\rho$, solid curve), O density secular variation (short dashed curve), and O density fluctuation (dotted curve) at z = 100 km altitude as a function of time at the first horizontal grid position for wave 1. See text for details.

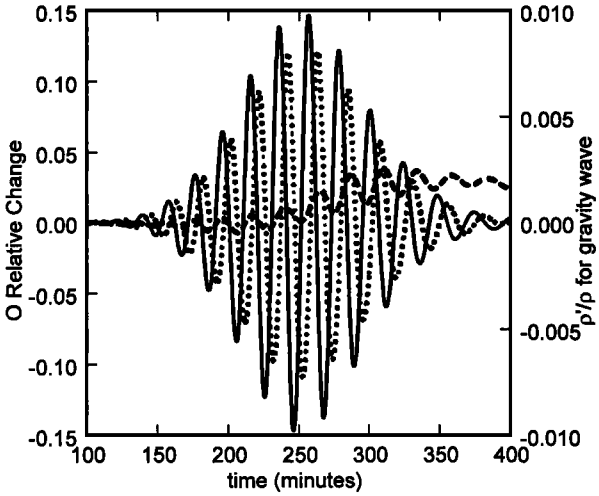

Figure 2b. Similar to Figure 2a except for wave 2.

the same amplitude as those shown here, but the phase will vary smoothly across the grid. Because the secular variation is an x-average, it does not vary with x.

The O column density (not shown) has a small secular variation associated with the destruction of O through three-body recombination reactions, mainly occurring on the bottom side of the O layer. Transport due to eddy diffusion and the wave-driven secular variation brings O down to this region where it recombines. When averaged over all model horizontal positions the O column density fluctuation is nil.

Figure 2b shows results similar to those for Figure 2a except for wave 2. This is a faster wave packet, and the disturbance first reaches the 100 km altitude level at times near 100 min. Maximum density perturbations at 100 km occur near 250 minutes (100 min sooner than for wave 1) with an amplitude of about 1 %. Because the individual Fourier components have twice the speed of the corresponding components associated with wave 1, the amplitude decay of the packet at times greater than 300 min occurs rapidly compared to that associated with wave 1. Relative fluctuations in n(O) are ~ 15 % (a factor of ~3 smaller than for wave 1). There is a secular increase of $n(O)$ (short dashed curve), in contrast to the decrease associated with wave 1 shown in Figure 2a. This is because wave 2 peaks at a higher altitude compared to wave 1, and is transporting O down from higher altitudes at a faster rate than it can transport it downward and away from the 100 km altitude level.

Figure 3 shows final altitude profiles of n(O) for several simulations (see caption). Wave 1 has a significant effect on the distribution of O (dashed-dotted curve). At altitudes above (below) ~97 km (the height of the original O peak) O densities decrease (increase). These effects increase by a factor of 2 when the amplitude (A) of wave 1 is increased by a factor of $\sqrt{2}$ (long dashed curve), as expected because nonlinear flux terms are proportional to A^2. The effect of wave 1 is to cause a general downward displacement of the entire O profile. The effect of wave 2 (short dashed curve) is to cause a downward transport of O from the region above ~110 km altitude to lower regions, which causes a small increase in O between about 95 and 106 km altitude. The effect of eddy diffusion only (thick small dashed curve) is small compared to the effects of the waves, and leads to a small decrease in O at all

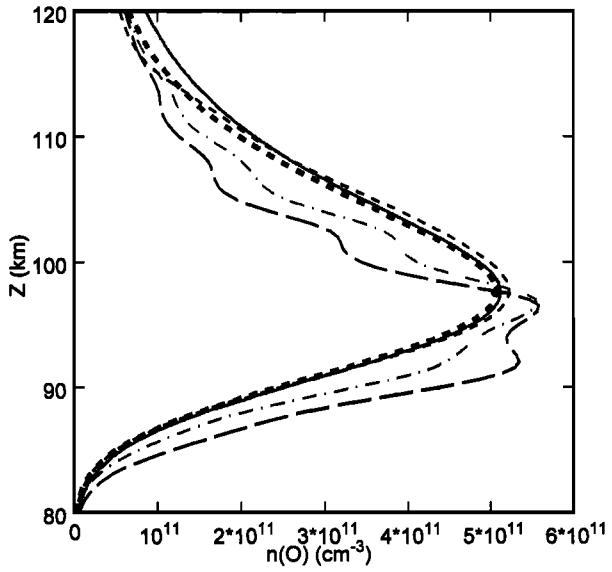

Figure 3. Final O profiles for different simulations. Initial profile (solid curve); effects of chemistry and eddy diffusion only, with η_{max} = 100 m^2 s^{-1} (thick small dashed curve); wave 1 at t = 500 minutes (dashed-dotted curve); wave 2 at t = 400 minutes (thin small dashed curve); and wave 1 at t = 500 minutes and amplitude increased by a factor of $\sqrt{2}$ (long dashed curve).

altitudes displayed. In contrast to the results obtained for wave 1, the shape of the O profile is not significantly affected and the altitude of peak O density remains unchanged, for either wave 2 forcing or for eddy diffusion acting alone. For $z \geq$ 120 km, n(O) is relatively insensitive to the particular wave parameters used in the simulations because transport due to molecular diffusion begins to dominate.

4.0 Conclusions

We have described a new model describing the time-dependent, non-linear response of the minor species to dynamical forcing by a gravity wave packet. We find that in addition to causing O fluctuations, the waves cause a large secular variation of O driven by wave transience and dissipation that is greatest for the slower wave packet that dissipates strongly below ~110 km altitude. The effects of eddy diffusion, with η_{max} = 100 m^2 s^{-1}, appear to be far less important than wave effects on the distribution of O in the MLT region. The transport effects considered here will need to be incorporated into future global scale models (using parameterization schemes) in order to accurately determine the O distribution in the MLT region.

Acknowledgements. MPH was supported by NSF Grant ATM-9816159, RLW was supported by NASA Grant NAG5-9193, and PGR was supported by NSF Grant ATM9815108.

5.0 References

Andrews, D. G., and M. E. McIntyre, Planetary waves in horizontal and vertical shears: the generalized Eliassen and Palm relation and the mean zonal acceleration, *J. Atmos. Sci., 33*, 2031-2048, 1976.

Banks, P. M., and G. Kockarts, *Aeronomy*, Academic Press, New York, 1973.

Burstein, S. Z., Finite-difference calculations for hydrodynamic flows containing discontinuities, *J. Comp. Phys., 2*, 198-222, 1967.

Eliassen, A., and E. Palm, On the transfer of energy in stationary mountain waves, *Geophys. Publ., 22*(3), 1-13, 1961.

Garcia, R. R., and S. Solomon, The effect of breaking gravity waves on the dynamics and chemical composition of the mesosphere and lower thermosphere, *J. Geophys. Res., 90*, 3850-3868, 1985.

Gardner, C. S., and Y. Zhao, Dynamic transport of mesospheric constituents by dissipating gravity waves: Na flux observations at Starfire Optical Range, New Mexico, *J. Geophys. Res., submitted*, 2000.

Hickey, M. P., G. Schubert, and R. L. Walterscheid, Gravity wave-driven fluctuations in the O_2 Atmospheric (0-1) nightglow from an extended, dissipative emission region, *J. Geophys. Res., 98*, 13,717-13,730, 1993.

Hickey, M. P., et al., A numerical calculation of gravity waves imaged over Arecibo during the 10-day January 1993 campaign, *J. Geophys. Res., 102*, 11,475, 1997.

Hickey, M. P., M. J. Taylor, C. S. Gardner, and C. R. Gibbons, Full-wave Modeling of Small-Scale Gravity Waves Using Airborne Lidar and Observations of the Hawaiian Airglow (ALOHA-93) O(^{1}S) Images and Coincident Na wind/temperature Lidar Measurements, *J. Geophys. Res., 103*, 6439, 1998.

Hickey, M. P., and R. L. Walterscheid, A Note on Gravity Wave-Driven Volume Emission Rate Weighted Temperature Perturbations Inferred from O_2 Atmospheric and O I 5577 Airglow Observations, *J. Geophys. Res., 104*, 4279, 1999.

Hickey, M. P., R. L. Walterscheid, and G. Schubert, Gravity wave heating and cooling in Jupiter's thermosphere, *Icarus, in press*, 2000.

Orlanski, I., and K. Bryan, Formation of thermocline step structure by large amplitude internal gravity waves, *J. Geophys. Res., 74*, 6975-6983, 1969.

Schoeberl, M. R., D. F. Strobel, and J. P. Apruzese, A numerical model of gravity wave breaking and stress in the mesosphere, *J. Geophys. Res., 88*, 5249-5259, 1983.

Schubert, G., R. L. Walterscheid, and M. P. Hickey, Gravity wave-driven fluctuations in OH nightglow from an extended, dissipative emission region, *J. Geophys. Res., 96*, 13,869-13,880, 1991.

Strobel, D. F., Parameterization of linear wave chemical transport in planetary atmospheres by eddy diffusion, *J. Geophys. Res., 86*, 9806-9810, 1981.

Strobel, D. F., Constraints on gravity wave induced diffusion in the middle atmosphere, *Pure Appl. Geophys., 130*, 533-546, 1989.

Torr, D. G., The photochemistry of the upper atmosphere, in *The Photochemistry of Atmospheres*, ed., Academic Press, Inc., 1985.

Walterscheid, R. L., Gravity wave mean state interactions in the upper mesosphere and lower thermosphere, in *The Upper Mesosphere and Lower Thermosphere: A Review of Experiment and Theory*, ed. M. Johnson and T. L. Killeen, Geophysical Monograph 87, American Geophysical Union, 1995.

Walterscheid, R. L., and G. Schubert, Gravity wave fluxes of O_3 and OH at the nightside mesopause, *Geophys. Res. Lett., 16*, 719-722, 1989.

Walterscheid, R. L., and W. K. Hocking, Stokes diffusion by atmospheric internal gravity waves, *J. Atmos. Sci., 48*, 2213-2230, 1991 1991.

Weinstock, J., Gravity wave saturation and eddy diffusion in the middle atmosphere, *J. Atmos. Terr. Phys., 46*, 1069-1082, 1984.

M.P. Hickey, Department of Physics and Astronomy, Clemson University, Clemson, SC 29634-0978. (e-mail: hickey@hubcap.clemson.edu)

R.L. Walterscheid, Space Science Application Laboratory, The Aerospace Corporation, Los Angeles, CA 90009.

P.G. Richards, Computer Science Department and Center for Space Plasma, Aeronomy, and Astrophysics Research, The University of Alabama in Huntsville, Huntsville, AL 35899.

(Received June 26, 2000; accepted August 18, 2000.)